Magnetism and decarburization-like diffusion process on V_2O_5-doped ZnO ceramics

Sion Federico Olive-Méndez, Carlos Roberto Santillán-Rodríguez, Karla Campos-Venegas, José Andrés Matutes-Aquino, Francisco Espinosa-Magaña

Abstract

We report on vanadium-doped ZnO ceramics to be used as sputtering targets. Prior to a sintering process, ZnO and V_2O_5 powders were milled in stoichiometric proportion to obtain Zn0.95V0.05O1 þδ composition. Sintering process of compressed powders was carried out at 900, 1000 and 1100 °C in air for 1, 2, 4, 6, 10 and 14 h. During the sintering process, decarburization-like diffusion of V_2O_5 (i.e. reduction of the V concentration in the pellet) leads to a non-homogeneous distribution of V. The solution of second Fick's law for a decarburization process $C(z,t) = (C_0 - C_S)erf\,(z/2\sqrt{\delta D_{gbt}}) + C_s$ was used to find δD_{gb}, where D_{gb} is the grain boundary diffusion coefficient and δ the grain boundary width. δD_{gb} strongly depends on sintering time, given that ZnO grain growth is accomplished with a simultaneous reduction of high diffusivity paths. X-ray diffraction analysis shows that residual V_2O_5 react with ZnO to produce γ-$Zn3(VO_4)_2$ and ZnV_2O_4 secondary phases that nucleate during cooling in interstitial sites between ZnO grains. Energy Dispersive X-Ray Spectroscopy (EDS) analysis was used to obtain vanadium concentration profiles. No

vanadium was observed in the lattice of ZnO grains, the only diffusion mechanism corresponds to Harrison's C-type kinetics. Ceramics exhibit a very low magnetization, reaching a maximum saturation magnetization M_s=14.6*10^{-3} emu/cm^3 on the sample annealed at 1100 °C for 1 h. Magnetic signals are originated at the interface between the V-based secondary phases and ZnO grains, where a composition near to $Zn_{0.95}V_{0.05}O$ is obtained.

Introduction

Much work has been devoted to the study of diluted magnetic oxides (DMO), which are large band gap oxides (ZnO, SnO_2, TiO_2, etc.) doped with 3d transition metals, mainly V, Mn, Co, Fe and Ni, in order to explain the origin of ferromagnetic order [1,2]. In DMO, the ferromagnetic order is produced by the alignment of the magnetic moment of the 3d cations within a hydrogenic orbital of an electron trapped in an F-center (anion vacancy corresponding to an oxygen vacancy in oxides). The principal application of DMO lies on spintronics, a particular topic of microelectronics, which combines the charge and the spin of electrons to create new physical phenomena [3]. Fabrication of spintronic devices is based on thin film technology where sputtering and pulsed laser deposition are the main industrial synthesis techniques used for thin film elaboration. Several works have been devoted to the study of V-doped ZnO ceramics, nanoparticles and thin films [4–12] but only a few reports of magnetic

properties on this system can be found in the literature. In a previous work we found that 5 at% V-doped ZnO nanoparticles [8] exhibit a saturation magnetization of $22.4*10^{-3}$ emu/cm3 while other groups report the absence of magnetic order in ZnO single crystals [13] and nanoparticles [14]. We focus on the elaboration of V-doped ZnO ceramics to be used as sputtering targets for further thin film elaboration. A homogeneous distribution of V on the ZnO target is imperative in order to obtain reproducible V content on the films. The homogeneous distribution of V needs to overcome the solubility limit of V on ZnO, which is 0.28 mol% and that decrease to 0.18 mol% when sintering temperature decreases from 850 to 750 °C.

In this paper we report the grain boundary diffusion coefficients (δD_{gb}) depending on sintering time, at different temperatures. The magnetic remanence, coercivity and saturation magnetization of the ceramics were also examined showing dependence with the extension of the interface between ZnO grains and ZnO-V secondary phases.

Experimental procedure

Samples were prepared using high purity ZnO 99.9% and V_2O_5 99.99% powders from Sigma-Aldrich. Appropriate proportions were thoroughly mixed in a high-energy SPEX D8000 mill using yttrium-stabilized zirconia balls and a nylon jar. The composition was fixed to $Zn_{0.95}V_{0.05}O_{1þδ}$. Powders were isostatically pressed under 90 MPa without any binder addition and green density of 3.39 g/cm3. Compressed powder samples were positioned in an alumina crucible and buried with alumina powder to promote

uniform heat transfer from the furnace. Sintering was performed at 900, 1000 and 1100 °C for 1, 2, 4, 6, 10 and 14 h in air atmosphere. Relative density of all samples after sintering is about 94–96%. Dimensions of the obtained pellets were 4 mm in height and 8 mm in diameter. X-ray diffraction (XRD) patterns were obtained with a Philips, PANalytical X'Pert equipment producing CuKα radiation (λ=1.54 Å). Average grain size and grain morphology was obtained using a scanning electron microscope Jeol JSM 5800-LV. Energy Dispersive X-ray Spectroscopy (EDS) from EDAX, was used to obtain vanadium concentration along the longitudinal z axis, at the top surface (z=2 mm) and at the center of the pellet (z=0 mm), see inset in Fig. 3. Better accuracy was obtained from EDS analysis performed in top view at z=0 and 2 mm.

Results and discussion

-V_2C_5 decarburization-like diffusion on ZnO

Structural characterization was carried out by X-ray diffraction on all samples, Fig. 1 shows the XRD patterns of samples annealed at 900, 1000, and 1100 °C for 1 and 14 h, the diffraction patterns of samples annealed for 2, 4, 6 and 10 h show similar features. All the diffraction patterns exhibit the hexagonal wurtzite structure of ZnO. Low-intensity peaks at 28.131 and 291 correspond to γ-$Zn_3(VO_4)_2$ and the peak at 42.751 corresponds to ZnV_2O_4 secondary phases[15]. These phases appear when sintered at low temperature (900 °C) or at a higher temperature (1000 °C) for short time periods ≤6 h. These phases are present in samples annealed at higher temperatures

and/or longer sintering time but the wt% concentration on the pellet is lower than the XRD limit detection to produce significant diffraction. According to the V_2O_5–ZnO phase diagram [16] these secondary phases are in solid state at temperatures lower than 900 °C, revealing that reaction between V2O5 and ZnO occurs during the pellet cooling process and not during sintering.

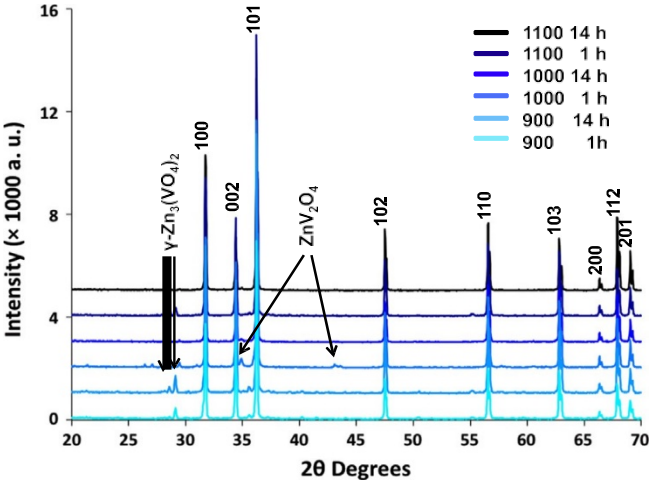

Fig. 1. XRD patterns for samples sintered at 900, 1000 and 1100 1C for 1 and 14 h. Secondary phases γ-$Zn_3(VO_4)_2$ and ZnV_2O_4 are found on samples sintered at low temperature (900 1C) and for short sintering time 1–6h at 1000 1C.

Furthermore, V_2O_5 melting point is 690 °C, thus during sintering V_2O_5 remains in liquid phase and secondary phases nucleate in interstitial sites between ZnO grains during the cooling process.

SEM micrographs of samples sintered at 1100 1C for 1, 2, 4, 6, 10 and 14 h are shown in Fig. 2. The average grain-size evolution can be fitted with the kinetic expression $G = k\sqrt[n]{te^{cT}}$ which is time dependent for a given temperature [17]. The size

of the initial ZnO powders (after ball-milling and prior to sintering, measured using Scherrer formula from XRD patterns) was 45 nm, where the V_2O_5 nanoparticles were homogeneously distributed and probably with smaller size as no diffraction signal was observed. However, careful EDS examination at high SEM magnifications of the sintered ZnO:V_2O_5 ceramics, reveals that ZnO grains do not contain V atoms, discarding V lattice diffusion into ZnO grains. Similar behavior has been reported on densification of ZnO ceramics adding SiO_2, where SiO_2 diffuses toward the ZnO grain surface [18].

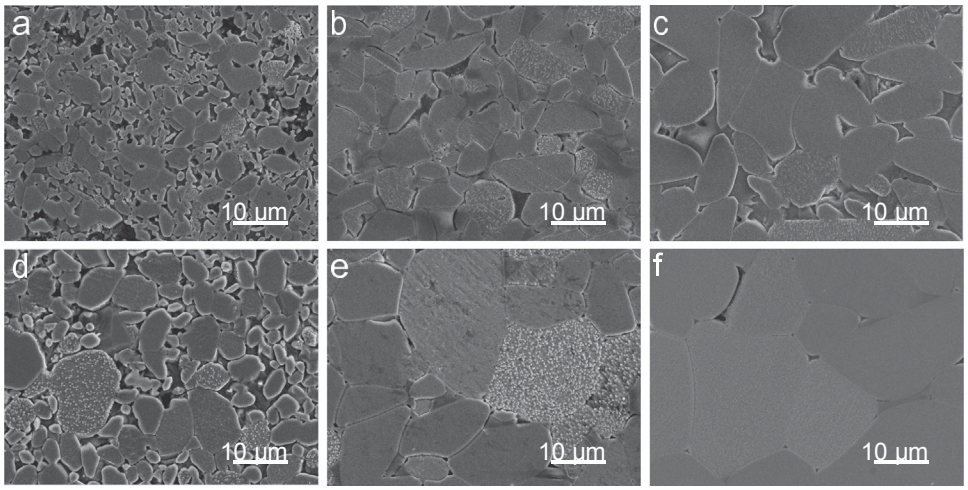

Fig. 2. SEM micrographs showing the grain growth evolution for sintering at 1100 °C. the average grain sizes are 15, 25.3, 28.4, 32, 35.2 and 37.3 mm for sintering periods of (a) 1 h, (b) 2 h, (c) 4 h, (d) 6 h, (e) 10 h and (f) 14 h, respectively.

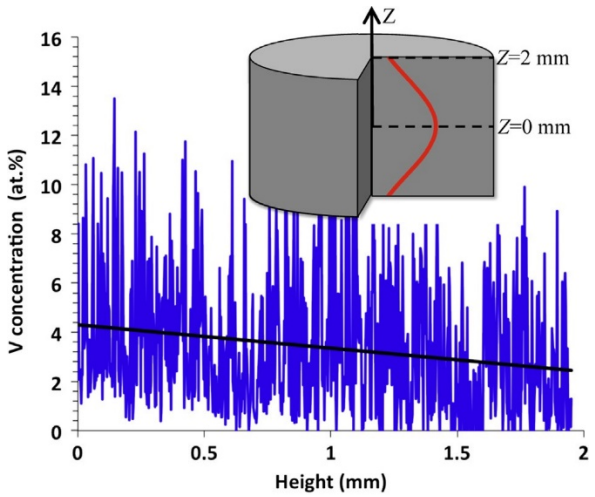

Fig. 3. EDS Line profile obtained from a pellet sintered at 1100 °C for 1 h. The high noise-to-signal ratio and the variation of the V concentration are attributed to the inhomogeneous distribution of the grain boundaries compared to the EDS probe size. Inset shows a theoretical C(z,t) profile along the z axis and the z=0 and 2 mm positions where top-view EDS was collected.

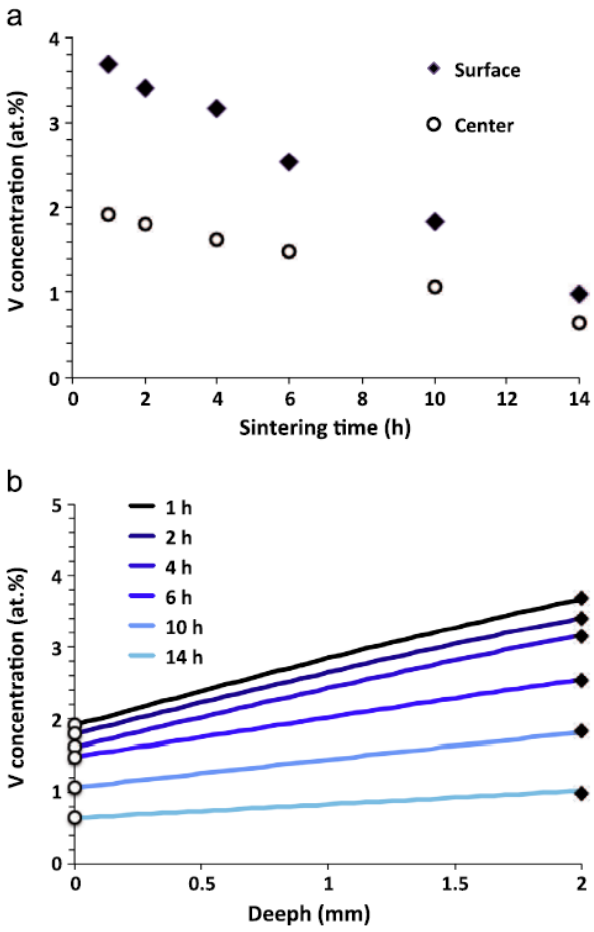

Fig. 4. (a) Punctual EDS data collected at $z=2$ mm (top surface) and $z=0$ mm (center) of the pellet for samples sintered at 1100 °C for 1, 2, 4, 6, 10 and 14 h. (b) EDS Data plotted against z position, the continuous lines correspond to the fit of Eq. (1) to find δD_{gb}.

Fig. 3 shows a line profile scan along z direction (see inset in Fig. 3) of a sample sintered at 1100 °C for 1 h. Due to the inhomogeneous distribution of the diffusivity paths and the punctual character of the EDS probe, a large noise-to-signal ratio and fluctuations around the expected V concentration make the line profile difficult to be fitted by Eq. (1) with the possibility of introducing a large error on the data interpretation. This difficulty motivated us to look for an alternative option. The inset in Fig. 3 shows a

schematic representation of the pellet depicting a theoretical concentration profile C(z,t) along z direction, the maximum concentration should be found at z=0, while lower concentrations must appear at the top (z=2 mm) and bottom (z=-2 mm) surfaces. After the sintering process, V concentration at z=0, should be less than C_0 which is the initial V concentration (i.e. 5 at%). To obtain EDS spectra at z=0 samples were polished to remove the top material until z=0 mm was reached. Top view EDS acquisition at low SEM magnification was performed at z=0, and z=2 mm.

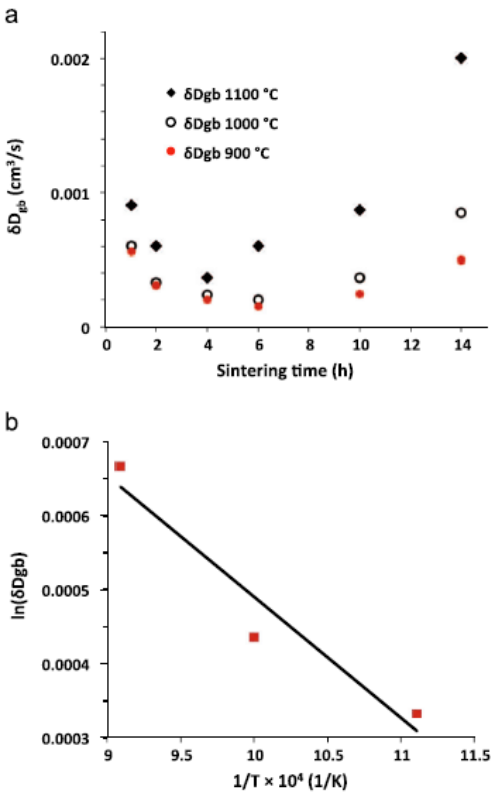

Fig. 5. (a) δD_{gb} values for all samples. (b) Arrhenius plot of the average δD_{gb} for each temperature used to find D^0_{gb}=1:0021 cm3/s and activation energy ΔH_{gb}=1.66*10^{-3} J mol^{-1}.

A compilation of V concentrations for samples sintered at 1100 °C obtained at z=0 and 2 mm is shown in Fig. 4a, similar graphs were obtained for sintering at 900 and 1000 °C. These values exhibits a linear trendline with sintering time, however, this data cannot be exploited by equating the slope of the fitted line with the derivative of Eq. (1) as the boundary conditions C(0,0)=5 at% and C(2,0)=5 at% are not satisfied. To determine the grain boundary diffusion coefficients (δD_{gb}), first we discard A and B-type kinetics as no V was found in the ZnO grains (i.e. no lattice diffusion occurred during the sintering process). Therefore diffusion occurs exclusively through grain boundaries, corresponding to C-type kinetics [19] defined by Harrisons conditions [20]. The solution of C-type kinetics uses second's Fick law, with a slight modification as the V concentration at any point decreases with time and concentration increases when moving towards the interior of the sample (i.e. increasing z) then cerf function is changed by erf function. Instead of only calculating D_{gb} coefficient, which depends on the width of the grain boundary δ=0.5 Å [21], it is used to calculate δD_{gb}. The data points of Fig. 4a were then plotted against the height z on Fig. 4b and the δD_{gb} was obtained using the equation:

$$\frac{C(x,t)-C_s}{C_0-C_s} = erf\left(z/2\sqrt{\delta D_{gb} t}\right) \qquad (1)$$

where C_s is the V concentration at the surface of the pellet for a given sintering time t>0, and C_0 is the initial V concentration at t=0. It is important to note that any value obtained at z=0 mm reaches a V concentration of 5 at% demonstrating that diffusion occurs very fast. Graphs with the same nature of Fig. 4b were made for the sintering process at 1000 and 900 °C. Fig. 5a depicts all δD_{gb} values for all sintering temperatures. An important issue is that the density of high diffusivity paths is not constant with sintering time, due to the increase of grain size. A minimum of δD_{gb} vs time is observed on Fig. 5a for sintering periods of 4–6 h attributed to an abrupt increase of grain size and also to the remaining amount of liquid V_2O_5, which acts as a diffusion barrier limiting the decarburization diffusion-like process on the ZnO ceramics.

The average values of δD_{gb} obtained from Fig. 5a for each temperature were used to create an Arrhenius plot of $\ln(\delta D_{gb})$ against the reciprocal temperature (1/T) as shown in Fig. 5b.

The equation of the kinetics of the δD_{gb} against the temperature is represented by the equation:

$$\delta D_{gb} = D_{gb}^{0} \exp(-\Delta H_{gb}/RT) \qquad (2)$$

where D0, ΔH, R and T are the pre-exponential factor, activation energy, gas constant and temperature, respectively. The ln function applied to Eq. (2) allows us to obtain the slope of the linear fit and the interception point with the vertical axis as follows:

$$\ln(\delta D_{gb}) = \ln\left(D^0_{gb}\right) - \Delta H_{gb}/RT \qquad (3)$$

The pre-exponential factor is D^0_{gb}=1.0021 cm3/s and is found to be four orders of magnitude larger than that of oxygen tracer lattice diffusion on ZnO ceramics. On the other hand, the activation energy $\Delta H_{gb}=1.66*10^{-3}$ J mol^{-1} is 6 orders of magnitude smaller than that of oxygen tracer on ZnO [22]. Here ΔH_{gb} represents the necessary energy that V_2O_5 molecules require to move through a grain boundary.

-Magnetic Properties

The room temperature M(H) magnetic loops of samples sintered at 900, 1000 and 1100 °C for 1 h are shown in Fig. 6. The highest saturation magnetization, after subtraction of the diamagnetic component of ZnO, $M_s=14.6*10^{-3}$ emu/cm3 was obtained for the highest sintering temperature, which decreases to 0.22 10-3 emu/cm^3 when sintering for 14 h. Despite the reduction of grain boundaries at 1100 °C, we suggest that V-ZnO based secondary phases are better distributed surrounding the ZnO grains and that a perfect DMO is formed at the ZnO grain surface producing ferromagnetic order. Inset 1 in Fig. 6 corresponds to the M(H) loops before subtraction of the diamagnetic component of pure ZnO that corresponds to ~99.99 wt% of the total weight of each sample, thus only ~0.01 wt% of the sample is responsible of the ferromagnetic signal. Inset 2 shows a closer look of the M(H) loops near the origin to evaluate coercivity and

remanence of the measured samples. Coercivity is ~80 Oe and magnetic remanence reaches $4*10^{-3}$ emu/cm^3 ensuring ferromagnetic order without the necessity of an external magnetic field. These non-zero values are typical of DMO and demonstrate that percolation of the BMPs is ensured through the grain boundaries. Another test to verify that the origin of the ferromagnetic order is the BMP, is to fit the experimental M(H) loops with the expression $M=M_s\tanh(H/H_a)$ where H_a is an effective saturation field [23]. In our samples H_a=2000 Oe, which perfectly fits the set of M_s and H_a found on other DMO systems [24]. Lower values of H_a, for similar values of M_s, like those of our measurements, are found on superparamagnetic systems.

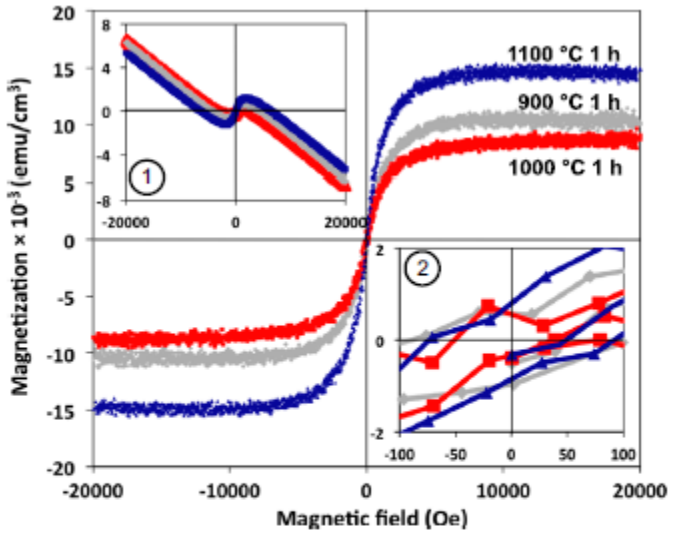

Fig. 6. Magnetic $M(H)$ loops for samples sintered at 900, 1000 and 1100 °C for 1 h. Inset 1 shows the $M(H)$ loops before the subtraction of the diamagnetic component from the pure ZnO grains. Inset 2 shows the small coercivity and remanence typical of DMO.

Conclusions

In this work we found the diffusion coefficients in a decarburization-like diffusion process during sintering of ZnO:V_2O_5 compressed powders. During sintering, ZnO grains grow at the same time that V_2O_5 diffuses toward the surfaces of the sample. Remaining V_2O_5 in the sample reacts with ZnO, during the cooling process, on the surface of grains at interstitial grain sites, leading to the formation of γ-$Zn_3(VO_4)_2$ and ZnV_2O_4 secondary phases. Grain boundary diffusion coefficients were found using second Fick's law for a C-type kinetics model, where no lattice diffusion is observed. The boundary conditions of the decarburization process use erf function instead of cerf on the solution of second Fick's law. We found that V_2O_5 acts as a diffusion barrier leading to minimum δD_{gb} for sintering periods of 4–6 h. From the Arrhenius plot of the average δD_{gb} with 1/T, the activation energy $\Delta H_{gb}=1.66*10^{-3}$ J mol^{-1} and the pre-exponential factor D^0_{gb}=1:0021 cm^3/s were found. The largest magnetization $M_s=14.6*10^{-3}$ emu/cm^3 was found for the sample annealed at 1100 °C which decreases with increasing sintering time. Ferromagnetic order exists at the grain boundaries of the ceramics through the percolation of BMPs. Sintering at 1100 °C for short time periods is recommended for ZnO:V target fabrication.

Acknowledgments

Authors are grateful to the technical assistance of Miguel Humberto Bocanegra Bernal for pellets compression and also to the financial support received from the Fondo Mixto Chihuahua (FOMIX) Grant no. CHIH-2009-C02-125921.

References

[1] Y. Kimishima, M. Uehara, K. Irie, S. Ishihara, T. Yamaguchi, M. Saitoh, K. Kimoto, Y. Matsui, Production of bulk dilute ferromagnetic semi- conductor by mechanical milling, J. Magn. Magn. Mater. 320 (2008) e674–e677.

[2] Q. Wang, Q. Sun, P. Jena, Y. Kawazoe, Dependence of magnetism on doping concentration in V-doped bulk ZnO, Mater. Trans. 49 (2008) 2469–2473.

[3] T. Zhao, S. R. Shinde, S. B. Ogale, H. Zheng, T. Venkatesan, R. Ramesh, S. Das Sarma, Electric field effect in diluted magnetic insulator anatase Co:TiO_2, Phys. Rev. Lett. 94 (2005) 126601.

[4] P. Amézaga-Madrid, W. Antúnez-Flores, J. E. Ledezma-Sillas, J. G. Murillo-Ramírez, O. Solís-Canto, O. E. Vega-Becerra, R. Martínez-Sánchez, M. Miki-Yoshida, Synthesis, microstructural characterization and optical properties of undoped, V and Sc doped ZnO thin films, J. Alloy. Compd. 509 S (2011) S490–S495.

[5] M. E. Koleva, P. A. Atanasov, N. N. Nedialkov, H. Fukuoka, M. Obara, Role of vanadium content in ZnO thin films grown by pulsed laser deposition, Appl. Surf. Sci. 254 (2007) 1228–1231.

[6] K. Lovchinov, H. Nichev, O. Angelov, M. Sendova-Vassileva, V. Mikli, D. Dimova-Malinovska, Structural, optical and electrical properties of V doped ZnO thin films deposited by r.f. magnetron sputtering, J. Phys.: Conf. Ser. 253 (2010) 012030.

[7] W. Li-Wei, X. Zheng, M. Li-Jian, V. Teixeira, S. Shi-Geng, X. Xu-Rong, Influence of concentration of vanadium in zinc oxide on structural and optical properties with lower concentration, Chin. Phys. Lett. 26 (7) (2009) 077801.

[8] S.F. Olive-Méndez, C.R. Santillán-Rodríguez, R.A. González- Valenzuela, F. Espinosa-Magaña, J.A. Matutes-Aquino, Role of vanadium ions, oxygen vacancies, and interstitial zinc in room temperature ferromagnetism on ZnO–V_2O_5 nanoparticles, Nanoscale Res. Lett. 9 (2014) 169.

[9] M. Mirzayi, M.H. Hekmatshoa, Effect of V2O5 on electrical and micro- structural properties of ZnO ceramics, Physica B. 414 (2013) 50–55.

[10] C.W. Zou, X.D. Yan, J.M. Bian, W. Gao, Enhanced visible photo- luminescence of V_2O_5 via coupling ZnO/V_2O_5 composite nanostructures, Opt. Lett. 35 (2010) 1145–1147.

[11] J.-J. Kim, T.-B. Hur, J.S. Kwak, D.Y. Kwon, Y.-H. Hwang, H.-K. Kim, Solubility of V2O5 in polycrystalline ZnO with different sintering conditions, J. Korean Phys. Soc. 47 (2005) S333–S335.

[12] J. Wu, T. Li, T. Qi, Q. Qin, G. Li, B. Zhu, R. Wu, C. Xie, Influence of dopants on electrical properties of ZnO–V_2O_5 varistors deduced from AC impedance and variable-temperature dielectric spectroscopy, J. Electron. Mater. 41 (7) (2012) 1970–1977.

[13] S. Zhou, K. Potzger, H. Reuther, K. Kuepper, W. Skorupa, M. Helm,

J. Fassbender, Absence of ferromagnetism in V-implanted ZnO single crystals, J. Appl. Phys. 101 (2007) 09H109.

[14] R. Dogra, M.R. Cordeiro, A.W. Carbonari, R.N. Saxena, M.S. Costa, Absence of room temperature ferromagnetism in transition metal doped ZnO nanocrystalline powders from PAC spectroscopy, Hyperfine Inter- act. 197 (2010) 77–81.

[15] H.H. Hng, K.M. Knowles, Characterization of Zn_3 (VO4)2 phases in V_2O_5-doped ZnO varistors, J. Eur. Ceram. Soc. 19 (1999) 721–726.

[16] M. Kurzawa, I. Rychlowska-Himmel, M. Bosacka, A. Blonska-Tabero, Reinvestigation of phase equilibria in the V_2O_5–ZnO system, J. Therm. Anal. Calorim. 64 (2001) 1113–1119.

[17] H.H. Hng, L. Halim, Grain growth in sintered ZnO mol 1% V_2O_5 ceramics, Mater. Lett. 57 (2003) 1411–1416.

[18] N. Canikoğlu, N. Toplan, K. Yildız, H.Ö. Toplan, Densification and grain growth of SiO_2-doped ZnO, Ceram. Int. 32 (2) (2006) 127–132.

[19] J.C. Fisher, Calculation of diffusion penetration curves for surface and grain boundary diffusion, J. Appl. Phys. 22 (1951) 74.

[20] L.G. Harrison, Influence of dislocations on diffusion kinetics in solids with particular reference to the alkali halides, Trans. Faraday Soc. 57 (1961) 1191–1199.

[21] J. Sommer, C. Herzig, Direct determination of grain-boundary and dislocation self-diffusion coefficients in silver from experiments in type-C kinetics, J. Appl. Phys. 72 (1992) 2758.

[22] I. Sakaguchi, K. Matsumoto, T. Ohgaki, Y. Adachi, K. Watanabe, N. Ohashi, H. Haneda, Oxygen tracer diffusion in magnesium-doped ZnO ceramics, J. Ceram. Soc. Jpn. 118 (2010) 362–365.

[23] K. Ackland, L.M.A. Monzon, M. Venkatesan, J.M.D. Coey, Magnetism of nanostructured CeO_2, IEEE Trans. Magn. 47 (2011) 3509–3512.

[24] J.M.D. Coey, J.T. Mlack, M. Venkatesan, P. Stamenov, Magnetization process in dilute magnetic oxides, IEEE Trans. Magn. 46 (2010) 2501–2503.